Published in final edited form as:
Nat Astron. 2020 January ; 4(1): 97–105. doi:10.1038/s41550-019-0899-4.

Prevalence of non-aromatic carbonaceous molecules in the inner regions of circumstellar envelopes

Lidia Martínez[#1], **Gonzalo Santoro**[#1], **Pablo Merino**[#1,2], **Mario Accolla**[1], **Koen Lauwaet**[3], **Jesús Sobrado**[4], **Hassan Sabbah**[5], **Ramón J. Pelaez**[6], **Victor J. Herrero**[6], **Isabel Tanarro**[6], **Marcelino Agúndez**[2], **Alberto Martín-Jimenez**[3], **Roberto Otero**[3], **Gary J. Ellis**[7], **Christine Joblin**[5,*], **José Cernicharo**[2,*], **José A. Martín-Gago**[1,*]

[1]Instituto de Ciencia de Materiales de Madrid (ICMM-CSIC). Structure of Nanoscopic Systems Group. C/Sor Juana Inés de la Cruz 3, 28049 Cantoblanco, Madrid, Spain

[2]Instituto de Física Fundamental (IFF-CSIC). Group of Molecular Astrophysics, C/Serrano 123, 28006 Madrid, Spain

[3]IMDEA Nanociencia, Ciudad Universitaria de Cantoblanco, 28049 Cantoblanco, Madrid, Spain

[4]Centro de Astrobiología (CAB, INTA-CSIC). Crtade Torrejon a Ajalvir km4, 28850 Torrejon de Ardoz, Madrid, Spain

[5]IRAP, Université de Toulouse, CNRS, CNES, 9 Av. du Colonel Roche, 31028 Toulouse Cedex 4, France

[6]Instituto de Estructura de la Materia (IEM-CSIC). Molecular Physics Department. C/Serrano 123, 28006 Madrid, Spain

[7]Instituto de Ciencia y Tecnología de Polímeros (ICTP-CSIC). C/Juan de la Cierva 3, 28006 Madrid, Spain

[#] These authors contributed equally to this work.

Abstract

Evolved stars are a foundry of chemical complexity, gas and dust that provides the building blocks of planets and life, and dust nucleation first occurs in their photosphere. Despite their importance, the circumstellar regions enveloping these stars remain hidden to many observations, thus dust formation processes are still poorly understood. Laboratory astrophysics provides complementary routes to unveil these chemical processes, but most experiments rely on combustion or plasma

[*]Corresponding should be addressed to: gago@icmm.csic.es, jose.cernicharo@csic.es, christine.joblin@irap.omp.eu.

Data availability. The data that support the plots within this paper and other findings of this study are available from the corresponding author upon reasonable request.

Competing interests. The authors declare no competing interests.

Author contributions. *In-situ* experiments in *Stardust* were performed by L.M, G.S, P.M, and M.Ac.; C.J. and H.S. performed LDI experiments. P.M.; K.L, R.O and A.M performed STM images. L.M. performed AFM images. RJ.P, V.J.H. and I.T. performed the OES experiments. M.Ag. made the kinetic calculations. G.J.E. and J.A.M-G wrote the first version of the manuscript. J.A.M-G supervised *in-situ* experiments, and C.J. and J.C the astrochemical interpretation. All authors discussed and contributed to the final version of the manuscript.

Europe PMC Funders Author Manuscripts

decomposition of molecular precursors under physical conditions far removed from those in space. We have built an ultra-high vacuum machine combining atomic gas aggregation with advanced *in-situ* characterization techniques to reproduce and characterize the bottom-up dust formation process. We show that carbonaceous dust analogues formed from low-pressure gas-phase condensation of C atoms in a hydrogen atmosphere, in a C/H_2 ratio similar to that reported for evolved stars, leads to the formation of amorphous C nanograins and aliphatic C-clusters. Aromatic species or fullerenes do not form effectively under these conditions, raising implications for the revision of the chemical mechanisms taking place in circumstellar envelopes.

Stars, like our Sun, in their final stages of evolution reach the asymptotic giant branch (AGB) accompanied by a massive ejection of matter containing the vast chemical complexity that provides the building blocks of planets and the main ingredients necessary for the emergence of life[1–3]. The advent of powerful radio-telescopes like ALMA, with improved radial resolution and sensitivity, opens the possibility to outline the basic physical and chemical conditions in which stardust is formed in the circumstellar envelopes (CSE)[4–6]. This dust, which consists of silicates or carbonaceous material depending on the C/O elemental abundance ratio of the AGB star, will then be ejected into the interstellar medium (ISM) where, after processing, it becomes involved in the formation of new stars and planets. However, the chemical nature of the dust seeds and carbonaceous molecules produced by C-rich evolved stars, as well as the chemical routes leading to them, is still controversial.

The dust seeds are first generated in the vicinity of the photosphere, at about 1-2 stellar radii[7]. In these regions, carbon nucleates into nanometer-sized grains in an equilibrium process with a low degree of ionization due to the absence of energetic radiation. The nucleation zone of an AGB star can be regarded as a homogeneous dense atomic cloud in the photosphere that, contrary to the outer layers, is devoid of UV photons. Physical parameters in nucleation zones remain uncertain because they are difficult to derive from observations[4]. Therefore, understanding the formation and nature of carbon stardust is complex and cannot be addressed solely by astronomical observations; dedicated laboratory simulations are required [8–15]. However, most experiments are unable to approach the relevant physical conditions, since they rely on energetic plasmas, combustion or decomposition of molecular precursors under conditions very unlike those in the dust formation regions of CSE[8].

A related issue is the formation of large carbonaceous molecules, polycyclic aromatic hydrocarbons (PAHs) and fullerenes. PAHs, identified by the emission of aromatic infrared bands (AIBs)[16], are widespread in regions of massive star formation and in C-rich protoplanetary and planetary nebulae. Buckminsterfullerene C_{60} has been detected in some of these environments[6,17,18,19]. A robust explanation of how these large molecules form is still lacking, especially in evolved stars where AIBs are only detected at late stages when the star evolves from red giant to white dwarf emitting ultraviolet (UV) radiation[20].

In this work, using a specifically designed ultra-high vacuum (UHV) experimental setup[21] we investigate the basic carbonaceous chemistry taking place in the dust formation region of CSEs. Our approach produces carbon dust seeds using exclusively gas-phase C atoms and

molecular hydrogen in a ratio close to that in the atmospheres of AGB stars without the requirement for introducing *ad hoc* C-bearing molecular precursors, such as acetylene or methane. Under these conditions, we show that nanosized carbon particles, pure carbon clusters and aliphatic carbon species are efficiently formed, whereas aromatics are only present at trace levels and no fullerenes are detected. Our results reproduce the relative abundances of simple molecules detected in CSEs, such as C_2H_2 and C_2H_4, which are directly generated by bottom-up chemistry and are simulated by a simple chemical kinetics model. Our data suggest that the pressures in circumstellar condensation environments are not sufficiently high for initiating cyclization mechanisms[22] and the formation of aromatic species must occur via other processes. We suggest that one pathway could be through thermal processing of aliphatic material on the surface of dust.

Results

Ultra-high vacuum gas aggregation sources for mimicking the dust formation region of CSEs

Our experimental set-up, called *Stardust*[21], is an UHV machine specifically conceived to simulate, with a high level of control, the complex conditions of stardust formation and processing in the environment of evolved stars. It uses UHV technology to avoid the high reactivity expected to atmospheric and residual gases of the formed carbon nanostructures[23]. A more detailed technical description is provided in Supplementary Information 1.

Many different techniques have been proposed to make dust analogues, each with advantages and limitations. In Supplementary table 1 we present a detailed critical compilation of the most commonly used techniques. Among them, laser ablation is one of the best suited [10], for instance, to simulate the reformation mechanisms of cosmic grains in the ISM[15]. In *Stardust,* we have chosen a sputter gas aggregation source (SGAS) because it is able to generate small clusters of nano-sized particles by gas-phase aggregation of individual atoms in a weakly ionized environment[24]. It is based on the vaporization of C atoms from a graphite target using Ar as the sputtering gas. Contrary to conventional standard magnetron sputtering [26,27], in SGAS nanoparticles and clusters form from gas phase reactions, as the sputtered material is trapped in the aggregation zone of the machine. Gas temperature during aggregation can be estimated to be < 1000 K[24], in the range of the condensation temperatures of solids in CSEs (500-2000 K)[7,25]. Thus, the chemistry proceeds via atom aggregation under conditions in which most of the reactions that occur are neutral-neutral, bimolecular and termolecular, closely resembling what happens in the dust formation region of CSEs.

In this work we unveil the formation of carbonaceous dust grains starting with a gas mixture containing the two most relevant species: carbon and molecular hydrogen. In carbon-rich CSEs, oxygen is locked into CO and SiO and therefore is not available to form dust [28,29]. Fig. 1 shows a pictorial representation of the CSE where typical carbon and hydrogen densities are provided. Supplementary table 2 further compares the conditions achieved in the gas aggregation zone with those in the dust formation zone of CSEs. Fig. 1b presents a scheme of *Stardust* in the configuration used for these experiments, which start with the vaporization of C atoms, followed by the injection of H_2. The C atoms react with H_2 and are

subsequently dragged through a nozzle by differential pressure into the next chambers, where they are either analysed in gas phase or collected on inert surfaces for further analysis. We have used different chemically-inert substrates to collect the carbonaceous stardust analogues for further studies, including Au, SiO_2 or graphite. The results we show hereafter are unaffected by the chosen substrate. Once the formed species pass the nozzle of the first chamber, no further growth takes place in the expansion.

The initial gas-phase vaporized C atoms may interact with residual or injected molecular hydrogen at different densities, and there are no other species involved except Ar (the residual density before magnetron operation, excluding Ar and H_2, is about 10^7 cm^{-3}). The vaporized C atoms have a density of about $2.5x10^{10}$ atoms·cm^{-3}, estimated from the sputtering energy (200 eV), the total drag current (200 mA) and the yield of emitted C atoms per impinging Ar^+ ion[30]. Under these conditions, sputtering of individual C atoms is preferential over C_2 and C_3[31]. Although the estimated value is some orders of magnitude higher than that accepted for the dust nucleation zones[28], it provides an effective method to accelerate the chemistry, which takes years in a real AGB envelope. Setting higher C densities together with an Ar overpressure, which accelerates the number of three-body reactions, are the two strategies adopted to overcome the exposure time limitation. Regarding hydrogen, we consider cases of low and high densities. In the first case, H_2 molecules and C atoms are in equal proportion, which can be achieved either using residual hydrogen or by introducing very low H_2 densities estimated in the range of 1.5×10^{10}mol·cm^{-3}, a value typically accepted for the dust nucleation zone at distances from the star of 2-3 R* [28]. In the second case, a high H_2 density is achieved by introducing extra hydrogen at a concentration estimated at 1.5×10^{12} mol·cm^{-3}, two orders of magnitude higher than that of vaporized C atoms. This situation provides a more appropriate concentration to simulate the chemistry in CSE in terms of H_2/C abundance (≈1000)[32].

Structure of the carbonaceous stardust analogues produced

Fig. 2a-b shows typical AFM images obtained from the C-dust collected on a surface. Two different morphological features can be identified. Firstly, carbonaceous nanosized grains (encircled in white in Fig. 2a) are efficiently produced as the most abundant constituents[10,15]. These spherical grains exhibit an extremely narrow size distribution with an average size of 9 nm (see Fig. 2a inset). Although larger grains (typically 100 nm) are thought to be present in space, in *Stardust* the nanoparticle size is conditioned by the geometry and experimental parameters and can be considered to represent the initial stages of carbonaceous dust growth. While the images of Fig. 2 were recorded for low hydrogen concentration, similar structures can be found for high H_2 densities.

Besides the carbonaceous nanograins, the other principal constituent of the C-dust analogues can be observed on the “flat” regions of Fig. 2b, where a thin mantle of material is observed, for instance in the area marked by a white square (see Supplementary Information 3). Structural resolution of these zones cannot be achieved using standard AFM, and more powerful *in situ* microscopies are required. Fig. 2c-d shows a scanning tunnelling microscope (STM) images obtained from the C analogues deposited on a Au surface. A STM-based detailed characterization of the imaged carbon products is complicated due to

the large number of different species generated and their sub-nanometric size. Fig. 2c shows a wide plethora of individual nanometer-sized structures at the surface, with apparent heights ranging from 1 to 5 Å that correspond to small amorphous C-clusters, but are difficult to ascribe to a particular cluster type. Some of these small molecules can self-assemble on the surface forming 2D ordered islands (see Fig. 2d). This process is surface-mediated suggesting electrostatic interactions between the molecules upon adsorption on surfaces. The structures forming the ordered regions are smaller than 8 Å and with a maximum apparent height of 0.6 Å (see inset). The small size suggests that they correspond to individual molecules containing only 3 to 5 C atoms. Unambiguous assignment to a precise chemical structure is difficult due to the fact that STM images show a topography convoluted with the electronic structure of the inspected element.

Aliphatic nature of the dust analogues

Swan C_2 lines are observed by Optical Emission Spectroscopy (OES) in the presence of low H_2 density, Fig. 3a, but are not found in the case of higher H_2 density. On the contrary, the H_α emission line is only seen at high H_2 density. These observations suggest that excited H atoms are generated during the chemical evolution, involving $C_2 + H_2 \rightarrow CCH + H$. The absence of the C_2 lines at high H_2 density indicates that most of the excited C_2 formed is consumed in this reaction. Interestingly, C_2 and H species are only detected in the regions close to the magnetron, which compares very well to observations from the photosphere of evolved stars where atomic hydrogen has been found and C_2 bands are prominent[33].

Fig. 3b presents the evolution of the masses of some relevant species during the experiment recorded at position QMS of Fig. 1b. The ON region in the figure corresponds to the time when the magnetron is switched on and the background values are obtained before and after this point. Although a direct assignment of the masses to their parent molecules is not straightforward due to the electron ionization that induces cracking patterns, we discuss the most important contribution for each mass observed. In the case of high H_2 densities, the predominant mass formed is 26 amu, mainly corresponding to C_2H_2 along with fragments of C_2H_4, C_2H_6 and larger aliphatic molecules. An increase of mass 16 amu is also observed, corresponding to methane. In the case of high H_2 densities, the formation of these species is more abundant and an increase is also detected in the main ionization fragments of ethane (C_2H_6), ethylene (C_2H_4), propane (C_3H_8) and larger alkanes, which later contribute to most of the masses. Importantly, in this work these species were formed directly from C atoms and molecular hydrogen, without introducing them as precursors, using ratios and aggregation processes similar to those reported for dust formation zones of CSEs[14]. Fig. 3b shows a decrease in the partial pressure of H_2 when C-evaporation is initiated, suggesting that in *Stardust* H_2 is partially consumed by chemical reactions. Neither benzene (78 amu) nor toluene (91 amu) are detected, indicating that they are below the detection limit (3×10^3 mol cm^{-3}). Interestingly, masses 18 and 32, corresponding to water and oxygen respectively, are unchanged with respect to their background pressure, indicating that, they are not involved in the reactions.

We have performed *ex-situ* laser desorption ionization mass-spectrometry (LDI-MS) in the so-called *AROMA* set-up [34], a machine with high sensitivity for PAH detection. Fig. 4

provides the ion distribution obtained by desorption/ionization of representative samples grown with both H_2 densities, showing that the molecular species generated have < 20 carbon atoms. C-clusters with a low degree of hydrogenation are observed for species containing 4 to 9 C atoms. Pure carbon clusters are observed from C_8^+ to C_{19}^+, and these are poorly hydrogenated above C_9^+, which can be understood by the formation of ring structures presenting lower reactivity[35]. Above 300 amu the signal completely vanishes, indicating the absence of fullerenes (see Supplementary Figure 4 for full mass range spectra).

The results from LDI-MS are summarized in the insets of Fig. 4 where the species are classified in families (see Supplementary Information 5 and methods). The analysis suggests a higher abundance of C_nH_m clusters for low H_2 density, indicating the formation of more saturated aliphatic species at higher H_2 density, which are not found by LDI-MS but evidenced by QMS (Fig. 3). Benzene or toluene, as key aromatic species, are marginally detected in both LDI-MS and QMS. With LDI-MS, a few aromatic species are evidenced in very low abundance (total of 3% for both H_2 densities), the largest being $C_{16}H_{10}$ (Fig. 4). Thus, it appears that the chemistry involved in the CSE does not favour the formation of PAHs, which can account for up to 18% of the total carbon species in the ISM[36].

Discussion

Kinetic and energetic modelling

We have constructed a time-dependent chemical kinetics model that computes the evolution of the chemical composition of a gas mixture. The model follows the formation of carbon-containing molecules from the precursor C + H_2, and aims to predict the principal molecules that can be formed and to understand the underlying chemical reactions behind their formation.

We use a gas-phase chemical network consisting of about 100 neutral and ionic pure carbon clusters and hydrocarbons containing up to 10 carbon atoms[37]. The initial conditions correspond to those of the high H_2 concentration experiment, and details are given in methods section.

In Fig. 5 we show the results of the calculations for some relevant species. It is seen that after several tens of seconds atomic carbon starts to be processed into different carbon-containing molecules. Pure carbon clusters such as C_3, unsaturated hydrocarbons like C_2H_2 and C_3H_2, and saturated hydrocarbons such as CH_4, C_2H_6, and C_3H_8 are abundantly formed. These results qualitatively agree with the molecules detected in the gas-phase (Fig. 3) in the *Stardust* machine, which indicates the disappearance of C_2 and the emergence of CH_4 and C_2H_2. According to the model, the molecular synthesis takes place in various steps.

The initial step, in which carbon is transformed from atoms to molecules, proceeds via three-body reactions with Ar as the third body. In particular,

$$C + C + Ar \; - - > C_2 + Ar$$

$$C + H_2 + Ar \rightarrow CH_2 + Ar$$

are key the reactions that constitute a bottleneck to the whole process of formation of C-containing molecules. For the pressure and temperature of the model, the time scale of these reactions is of the order of tens of seconds. The bimolecular reaction of atomic carbon with H_2 to produce CH + H is endothermic by about 100 kJ/mol and thus is not efficient at the considered temperature of 500 K.

Once the aforementioned starting reactions have formed the first molecular species, the growth of molecules is driven by bimolecular reactions and three-body reactions involving neutral species. Routes involving ions are less efficient under our experimental conditions. Moreover, reactions of hydrocarbons with Ar^+ are fast and result in fragmentation[38], which tends to produce a delay in molecular synthesis.

According to the model, carbon growth mainly occurs via insertion reactions of carbon atoms. For example, the reactions

$$C_2H_2 + C \rightarrow C_3 + H_2$$
$$\rightarrow C_3H + H$$

are fast[39] and drive the transformation from two carbon atoms to molecules with three C atoms. Analogous reactions of polyacetylenes with atomic carbon allow the progressive processing of carbon into aliphatic hydrocarbons of increasing complexity.

Apart from the increase in the number of carbon atoms, hydrogenation is also an important part of the chemical processing in the *Stardust* experiment. Hydrogenation essentially occurs via three-body reactions involving H atoms of the type

$$C_nH_x + H + Ar \rightarrow C_nH_{x+1} + Ar$$

in which H atoms are successively added. This way, CH_4 is formed from CH_2, and C_3H_8 from less hydrogenated species like C_3 and C_3H. Under our experimental conditions, H atoms are abundantly formed through various reactions involving ions like

$$Ar^+ + H_2 \rightarrow ArH^+ + H$$

There are some hydrogenation steps that mostly follow bimolecular reactions involving H_2 rather than three-body reactions involving H atoms. This is the case of the conversion of C_2 into C_2H, which occurs via the reaction

$$C_2 + H_2 \rightarrow C_2H + H$$

which could be rapid[40] and more efficient than the three-body reaction, C_2 + H + Ar.

The synthesis of hydrocarbons from atomic carbon is summarized in the scheme shown in Fig. 5. Carbon growth by C insertion and hydrogenation by three-body reactions with H can be extrapolated to larger species. However, the kinetics of reactions involving larger hydrocarbons is not so well constrained and it is likely that other routes, e.g., association of hydrocarbon fragments of different size, will also be efficient.

The calculations undertaken at different temperatures indicate that below 500 K (down to 300 K) the results are qualitatively similar to those obtained at 500 K, with little variation in the abundances caused by the dependence of the rate coefficients of the reactions involved in the molecular synthesis. At temperatures higher than 500 K the behavior gradually changes, with unsaturated hydrocarbons like polyacetylenic chains becoming more abundant at the expense of saturated hydrocarbons, like alkanes. At temperatures above 1000 K, the model predicts that alkanes should have negligible abundance. This suggests that there could be a turning point for temperatures around 800-1000 K. Below these temperatures, hydrocarbons with high H/C ratios would form efficiently whilst at higher temperatures C-bearing molecules with low H/C ratios would dominate. This may have implications for the formation of carbonaceous material in C-rich CSEs. At thermochemical equilibrium, graphite is predicted to condense at temperatures as high as 1500-2000 K[41]. However, the actual temperature at which carbonaceous dust forms in C-rich CSEs could be significantly lower because solid carbon may not be graphitic but rather in the form of less ordered materials like amorphous carbon[42] and because the process of condensation is probably controlled by chemical kinetics rather than by thermochemical equilibrium.

Thermal induced formation of aromatics on surfaces

Fig. 6 shows a representative mass spectrum single scan at 430K from an *in situ* TPD experiment. Although precise assignment of masses is difficult, families of C_nH_m hydrocarbons can be identified. The most abundant masses of 26 amu, 39 amu and 41 amu all belong to known fragments of larger aliphatic hydrocarbons[43]. Interestingly, benzene and naphthalene were observed exclusively after annealing the deposited carbon above 355K. These aromatic species are most likely formed after a catalytic recombination of small hydrocarbons on the gold surface, a process typically reported in surface chemistry[44,45]. Note that in the LDI-MS analysis, which is highly sensitive to aromatics, benzene was marginally observed whilst naphthalene was not detected. The fact that aromatics could be formed after annealing of carbonaceous aliphatics deposits on a C-rich surface needs to be further explored as a possible mechanism for the formation of these species in warm CSE environments. Indeed AIBs, the signature for PAHs, are not convincingly detected in AGBs but are observed at later stages when the star emits ultraviolet (UV) radiation that leads to photo-processing of the carbon-dust[20].

Astrophysical implications

There are several models to account for the presence of aromatic species in the ejecta of evolved stars; one involves the polymerization of acetylene to benzene[5] and further growth by the hydrogen abstraction acetylene addition (HACA) mechanism[22,46]. Other scenarios involve the processing of SiC dust grains[47] or the catalytic activity of C_2H_2 on silicate surfaces[48]. Although the HACA mechanism has been invoked to unravel the synthesis of

PAHs in the outflows of carbon-rich AGB stars[22,46], our results suggest an alternative scenario. We produce acetylene in a ratio C_2H_2/H_2 of 2×10^{-2}, compared to the 10^{-4} estimated for the inner layers of AGBs[4]. This is due to the fact that we have accelerated the chemistry by introducing higher C densities. Importantly, even under these favourable conditions we do not observe an efficient formation of PAHs. Earlier models of the formation of PAHs in CSE have shown that there is a narrow temperature window, between 900 and 1,100K, in which PAHs could form[22,49]. However, the conversion of benzene to larger PAHs was found to be a bottleneck in the reaction scheme. The role of shocked regions close to the star photosphere in which temperatures higher than 1,700 K could be reached have therefore been emphasized[50].

Our results also suggest the formation of a large amount of amorphous nanosized carbon grains that can be considered as the main component of the carbon stardust (see Fig. 3). Aliphatic species deposited on dust grains are susceptible to further reaction, between themselves in a catalytically activated process, leading to larger molecules or aromatic species upon thermal activation (see Fig. 6). Such a temperature rise could be achieved in the highly UV-irradiated environments of protoplanetary nebulae where polymerization of gas species and dust chemistry could also lead to the formation of PAHs[5,32].

Finally, we are able to qualitatively reproduce the abundances of the C_2H_2 and C_2H_4 found in CSEs around AGB stars, indicating that SGAS, a technique not previously used in laboratory astrophysics, can be a very valuable tool to gain information on the chemistry operating in CSEs. When compared to other techniques, SGAS more closely resemble the delicate conditions of these cosmic environments (see Supplementary table 2). Most of the previously used techniques lead to the formation of aromatics, in addition to grains and clusters, either because of the use of much higher temperatures or because of the use of very high pressures of acetylene.

Conclusions

The combination of laboratory astrophysics, surface science and astronomical observations can unveil the chemical routes that operate in the inner layers of the envelope of evolved stars, providing new insights into the chemistry of carbonaceous stardust seed formation and fostering new observations. Our results suggest that PAHs might not be efficiently form during gas-phase growth in the CSE, which we show to generate aliphatic material and C-clusters together with carbonaceous nano-sized grains. However, the species that are deposited on dust grains are susceptible to further processing and dust can catalyse the formation of aromatic species upon thermal activation, which could take place as a result of the significant rise in dust temperature that occurs in highly UV-irradiated environments.

Methods

Location of the experimental techniques in the Stardust machine

The composition of the small gas-phase species was analysed *in situ* by mass spectrometry (MS) and optical emission spectroscopy (OES). The material generated can be collected on a surface at position “sample-1” for *ex situ* studies, such as laser desorption ionization mass

spectroscopy (LDI-MS) or atomic force microscopy (AFM). Finally, the deposit (at position sample 2 in Fig.1) is characterized *in situ* in a third chamber by thermal programmed desorption (TPD).

Fabrication of the dust analogues

The carbon dust analogues were fabricated using a scaled-up multiple ion cluster source (MICS)[21], a type of sputtering gas aggregation source (SGAS), working under UHV conditions (base pressure 1×10^{-9} mbar) from Oxford Applied Research Ltd.. The magnetrons were loaded with a graphite target of 99.95% purity. The Ar flux used for the experiments was 150 sccm. The typical power applied to the magnetron was 100 W and the working aggregation length (distance between the magnetron and the exit nozzle) was 374 mm.

Extra-pure H_2 (99.99% purity) was injected during fabrication through one of the lateral entrances of the aggregation zone of the MICS (see Supplementary Figure 1), using gas-dosing valves with flux-regulator to inject into the UHV system. The doses used for these experiments were: 0, 4×10^{-4} and 1 sccm, with an Ar flux maintained at 150 sccm. The substrates employed for collecting the NPs are boron-doped Si(100) with its native oxide for AFM; polycrystalline Au for *AROMA* experiments; Au(111) and graphite for TPD analysis.

Atomic Force Microscopy (AFM)

measurements were performed in the dynamic mode using a Cervantes AFM System equipped with the *Dulcinea* electronics from Nanotec Electronica S.L. All images were analyzed using WSxM software[51]. AFM images were recorded *ex situ*.

Scanning tunnelling microscopy (STM)

Samples for scanning tunnelling microscopy (STM) were prepared in *Stardust* and transferred without exposing the samples to the atmosphere to the STM chamber, located in a different laboratory, using a UHV suitcase with an ion-getter pump (base pressure $<1\times10^{-9}$ mbar) to avoid chemical reaction with environmental gases[23]. This procedure can be considered as *in situ* since the surface has never reached a pressure higher than 10^{-9} mbar. Samples are deposited on an atomically flat single crystal Au(111) surface pre-cleaned by repeated sputtering/annealing cycles, which consisted of sputtering for 10 min using Ar^+ ions at an energy of 1.25 kV and subsequent annealing at 800 K for 5 min. Clean Au(111) is later exposed to the carbon analogues for 5 minutes keeping the sample at room temperature, then immediately transferred to the UHV suitcase and to the STM chamber. The total time between sample growth and insertion in the STM cryostat was limited only by the pumping of the load lock volume. STM measurements were performed at 4K in a LT-STM (Scienta Omicron) with a base pressure $<10^{-11}$ mbar.

Optical emission spectroscopy (OES)

The light emitted by the plasma generated in front of the magnetron was collected through a fused silica window and an optical fibre of fused silica, and analysed by OES (see position in Fig. 1a) using a 193 mm focal length, motorized Czerny-Turner spectrograph (Andor, model Shamrock SR-193-i-A) equipped with a CCD camera (iDus DU420A-BVF). Two

diffraction gratings with 1200 grooves/mm and 1800 grooves/mm, installed in a movable turret, provide spectral ranges of 300-1200 nm and 200-950 nm, respectively, and nominal spectral resolutions of 0.22 nm and 0.15 nm, respectively (for an input slit width of 20 μm). The relative spectral efficiencies of all the spectroscopic equipment was quantified for both diffraction gratings with a calibrated tungsten lamp.

In situ mass spectrometry (MS)

The gaseous species produced during the fabrication of the C-dust analogues were detected *in situ* with a quadrupole mass spectrometer (QMS) (0-100 amu) Prisma plus spectrometer from Pfeiffer. Lowest detectable partial pressure 10^{-10} mbar. The system includes a continuous secondary electron multiplier.

Laser desorption/ionization mass-spectrometry (LDI-MS): the *AROMA* setup

AROMA (Aromatic Research of Organics with Molecular Analyzer) is dedicated to the analysis, with micron-scale resolution, of the carbonaceous molecular content of cosmic dust analogues. The experimental setup consists of a microprobe laser desorption ionization chamber and a segmented linear quadrupole ion trap connected to an orthogonal time of flight mass spectrometer (LQIT-oTOF). For each detected m/z peak with a signal-to-noise ratio (S/N) greater than 10, a chemical formula was assigned using the mMass software[52], an open source mass spectrometry tool. The double bond equivalent (DBE) for each molecular formula was then calculated using the following equation for a given chemical formula of hydrocarbon species C_cH_h: DBE = c-(h/2)+1. This method allows sorting of the detected ions into families of compounds[53]. This is done using empirical factors that delineate DBE boundaries in complex natural organic matter[54]. Hydrocarbons with $0.5 < DBE/C < 0.9$ are considered to be aromatics. The line DBE/C ~1 corresponds to C clusters and the species falling in the zone $0.9 \leq DBE/C < 1$ are referred to as HC clusters, which includes C_cH_2 polyynes. Once all the detected species were sorted, the ion signal percentage was calculated for each family by dividing the sum of peak intensities detected in each family by the total ion intensity. The reported error bars in DBE analysis correspond to the relative standard deviation obtained for the total ion signal over a mass range of a family of compounds when the measurement was repeated several times (7 to 10) on natural samples. These error bars, of around 25%, are conservative since they have been derived from a complex matrix.

Thermal Programmed Desorption (TPD)

Experiments were performed *in situ* to determine the mass spectra of the carbon analogues deposited on low reactivity surfaces annealed at increasing temperatures. TPD was performed using a Pfeiffer HiQuad QMG 700 with QMA 400 mass spectrometer with a CP 400 ion counter preamplifier. The instrumentation allows measurement of masses between 0 and 512 amu with a detection limit of 10^{-15} mbar. After carbon analogue deposition the samples were placed in front of the quadrupole at a short distance (>1 cm) ensuring that the majority of the collected gas species derive from the surface of the sample surface. Atomically flat Au(111) and graphite substrates were used in the experiments, yielding comparable TPD spectra. Au(111) surfaces were cleaned *in situ* by the standard methodology of sputtering/annealing. Graphite was mechanically cleaved *ex situ* and

consecutively introduced into the vacuum system, which ensures an atomically fresh graphite surface prior to deposition. The carbon analogues were deposited during 100 minutes, ensuring that there is sufficient carbon material to obtain well-defined signals in the TPD experiments. A temperature ramp of 12.5°K·min^{-1} was applied from room temperature to the maximum temperature examined (700K).

Kinetic model

We use a gas-phase chemical network consisting of about 100 neutral and ionic pure carbon clusters and hydrocarbons containing up to 10 carbon atoms. These species are linked by about 2000 chemical reactions, whose rate constants are extracted from the literature on combustion chemistry, atmospheric chemistry, astrochemistry, as well as from specific chemical kinetics studies[37]. The starting composition of the gas consists of a mixture of Ar/Ar^+/H_2/H/C with mole fractions $1.0/10^{-4}/1.6\times10^{-6}/10^{-7}/2.6\times10^{-8}$. We consider that the gas is trapped in the aggregation zone at a constant pressure of 66 mbar (measured value) and a constant temperature of 500 K, which can be considered as an averaged representative value. In a second stage, the gas is neutralized and expands reaching a pressure of 0.1 mbar and a temperature of 300 K at a distance of 10 cm from the magnetron sources. At this stage, the sharp decrease in pressure makes the chemical reactions too slow in comparison with the dynamic time scale associated with the gas expansion, and the chemical composition remains quenched. Therefore, molecular synthesis takes place only during the first stage in the aggregation zone.

Supplementary Material

Refer to Web version on PubMed Central for supplementary material.

Acknowledgements

We thank the European Research Council for funding support under Synergy Grant ERC-2013-SyG, G.A. 610256 (NANOCOSMOS). Also, partial support from the Spanish Research Agency (AEI) through grants MAT2017-85089-c2-1R, FIS2016-77578-R and FIS2016-77726-C3-1-P is acknowledged. Support from the FotoArt-CM Project (P2018/NMT-4367) through the Program of R&D activities between research groups in Technologies 2013, co-financed by European Structural Funds, is also recognised.

References

1. Kwok S. The synthesis of organic and inorganic compounds in evolved stars. Nature. 2004; 430:985–991. [PubMed: 15329712]
2. Henning T, Salama F. Carbon in the universe. Science. 1998; 282:2204–2210. [PubMed: 9856936]
3. Meinert C, et al. Ribose and related sugars from ultraviolet irradiation of interstellar ice analogs. Science. 2016; 352:208–212. [PubMed: 27124456]
4. Fonfria JP, Cernicharo J, Richter MJ, Lacy JH. A Detailed Analysis of the Dust Formation Zone of IRC +10216 Derived from Mid-Infrared Bands of C_2H_2 and HCN. Astrophys J. 2008; 673:445–469.
5. Cernicharo J, et al. Infrared Space Observatory's Discovery of C_4H_2, C_6H_2, and Benzene in CRL 618. Astrophys J. 2001; 546:L123–L126.
6. Cami J, Bernard-Salas J, Peeters E, Malek SE. Detection of C_{60} and C_{70} in a young planetary nebula. Science. 2010; 329:1180–1182. [PubMed: 20651118]
7. Gail, H, Sedlmayr, E. Physics and Chemistry of Circumstellar Dust Shells (Cambridge Astrophysics). Cambridge: Cambridge University Press; 2013.

Europe PMC Funders Author Manuscripts

8. Schlemmer, S, Mutschke, H, Giesen, T, Jäger, C. Laboratory astrochemistry: From molecules through nanoparticles to grains. Wiley; 2014.
9. Kroto HW, Heath JR, O'Brien SC, Curl RF, Smalley RE. C_{60}: Buckminsterfullerene. Nature. 1985; 318:162–163.
10. Jäger C, Huisken F, Mutschke H, Jansa IL, Henning T. Formation of polycyclic aromatic hydrocarbons and carbonaceous solids in gas-phase condensation experiments. Astrophys J. 2009; 696:706–712.
11. Biennier L, et al. Characterization of circumstellar carbonaceous dust analogues produced by pyrolysis of acetylene in a porous graphite reactor. Carbon N Y. 2009; 47:3295–3305.
12. Pino T, et al. The 6.2 μm band position in laboratory and astrophysical spectra: a tracer of the aliphatic to aromatic evolution of interstellar carbonaceous dust. Astron Astrophys. 2008; 490:665–672.
13. Contreras CS, Salama F. Laboratory investigations of polycyclic aromatic hydrocarbon formation and destruction in the circumstellar outflows of carbon stars. Astrophys Journal, Suppl Ser. 2013; 208:6.
14. Peláez RJ, et al. Plasma generation and processing of interstellar carbonaceous dust analogs. Plasma Sources Sci Technol. 2018; 27
15. Fulvio D, Gobi S, Jaeger C, Kereszturi A, Henning T. Laboratory experiments on the low temperature formation of carbonaceous grains in the ISM. Astrophys J Suppl Ser. 2017; 233:14.
16. Peeters E, Spoon HWW, Tielens AGGM. PAHs as a tracer of star formation? Astrophys J. 2004; 613:986–1003.
17. Sellgren K, et al. C_{60} in reflection nebulae. Astrophys J. 2010; 722:L54–L57.
18. García-Hernández DA, et al. Formation of fullerenes in H-contaning planetary nebulae. Astrophys J Lett. 2010; 724:39–43.
19. Cordiner MA, et al. Confirming Interstellar C_{60}^{+} Using the *Hubble Space Telescope*. Astrophys J. 2019; 875:L28.
20. Kwok S, Zhang Y. Mixed aromatic-aliphatic organic nanoparticles as carriers of unidentified infrared emission features. Nature. 2011; 479:80–83. [PubMed: 22031328]
21. Martínez L, et al. Precisely controlled fabrication, manipulation and in-situ analysis of Cu based nanoparticles. Sci Rep. 2018; 8
22. Frenklach M, Feigelson ED. Formation of polycyclic aromatic hydrocarbons in circumstellar envelopes. Astrophys J. 1989; 341:372.
23. Ravagnan L, et al. Cluster-Beam Deposition and in situ Characterization of Carbyne-Rich Carbon Films. Phys Rev Lett. 2002; 89:285506. [PubMed: 12513160]
24. Haberland, H. Gas-Phase Synthesis of Nanoparticles. Huttel, Y, editor. Wiley-VCH; 2017. 3–21.
25. Lodders K, Fegley B. Condensation Chemistry of Circumstellar Grains. IAU Symp. 1999; 191:279–290.
26. Kratochvíl J, Kuzminova A, Kylián O, Biederman H. Comparison of magnetron sputtering and gas aggregation nanoparticle source used for fabrication of silver nanoparticle films. Surf Coatings Technol. 2015; 275:296–302.
27. Selwyn GS, Weiss CA, Sequeda F, Huang C. Particle contamination formation in magnetron sputtering processes. J Vac Sci Technol A Vacuum, Surfaces, Film. 1997; 15:2023–2028.
28. Agúndez M, et al. Molecular abundances in the inner layers of IRC +10216. Astron Astrophys. 2012; 543:A48.
29. Yang X, Chen P, He J. Molecular and dust features of 29 SiC carbon AGB stars. Astron Astrophys. 2004; 414:1049–1063.
30. Bueno RA, et al. Highly selective covalent organic functionalization of epitaxial graphene. Nat Commun. 2017; 8
31. Oyarzabal E, Doerner RP, Shimada M, Tynan GR. Carbon atom and cluster sputtering under low-energy noble gas plasma bombardment. J Appl Phys. 2008; 104
32. Cernicharo J. The Polymerization of Acetylene, Hydrogen Cyanide, and Carbon Chains in the Neutral Layers of Carbon-rich Proto-planetary Nebulae. Astrophys J Lett. 2004; 608:L41.

33. Contreras CS, Sahai R, de Paz AG, Goodrich R. Echelle long-slit optical spectroscopy of evolved stars. Astrophys J Suppl Ser. 2008; 179:166–194.
34. Sabbah H, et al. Identification of PAH Isomeric Structure in Cosmic Dust Analogs: The AROMA Setup. Astrophys J. 2017; 843:34. [PubMed: 28835724]
35. Van Orden A, Saykally RJ. Small Carbon Clusters: Spectroscopy, Structure, and Energetics. Chem Rev. 1998; 98:2313–2358. [PubMed: 11543299]
36. Joblin C, Leger A, Martin P. Contribution of polycyclic aromatic hydrocarbon molecules to the interstellar extinction curve. Astrophys J. 1992; 393:L79.
37. Agúndez M, Roueff E, Le Petit F, Le Bourlot J. The chemistry of disks around T Tauri and Herbig Ae/Be stars. A&A. 2018; 616
38. Anicich V. An index of the literature for bimolecular gas phase cation-molecule reaction kinetics. JPL Publ. 2003
39. Clary DC, et al. C + C_2H_2: A Key Reaction in Interstellar Chemistry. J Phys Chem A. 2002; 106:5541–5552.
40. Pitts WM, Pasternack L, McDonald JR. Temperature dependence of the C_2(X1Σg+) reaction with H_2 and CH_4 and C_2(X1Σg+ and a 3Πu equilibrated states) with O2. Chem Phys. 1982; 68:417–422.
41. Lodders, K, Fegley, B. Condensation chemistry of carbon starsAstrophysical implications of the laboratory study of presolar materials. Vol. 402. ASCE; 1997. 391–423.
42. Martin PG, Rogers C. Carbon grains in the envelope of IRC +10216. Astrophys J. 1987; 322:374.
43. Kramida, A, Ralchenko, Yu; Reader, J. NIST ASD Team. NIST Atomic Spectra Database (version 5.6.1). National Institute of Standards and Technology; Gaithersburg, MD: 2018. https://physics.nist.gov/asd.
44. Alyabyev SB, Beletskaya IP. Gold as a catalyst. Part II. Alkynes in the reactions of carbon–carbon bond formation. Russ Chem Rev. 2018; 87:984–1047.
45. Zaera F. Surface chemistry of hydrocarbon fragments on transition metals: Towards understanding catalytic processes. Catalysis Letters. 2003; 91:1–10.
46. Zhao L, et al. Pyrene synthesis in circumstellar envelopes and its role in the formation of 2D nanostructures. Nat Astron. 2018; 2:413–419.
47. Merino P, et al. Graphene etching on SiC grains as a path to interstellar polycyclic aromatic hydrocarbons formation. Nat Commun. 2014; 5
48. Tian M, et al. Catalytic conversion of acetylene to polycyclic aromatic hydrocarbons over particles of pyroxene and alumina. Philos Trans R Soc A Math Phys Eng Sci. 2013; 371doi: 10.1098/rsta.2011.0590
49. Cherchneff I, Barker JR, Tielens AGGM. Polycyclic aromatic hydrocarbon formation in carbon-rich stellar envelopes. Astrophys J. 1992; 401:269.
50. Cherchneff I, Cau P. The chemistry of carbon dust formation. IAU Symp. 1999; 191:251–260.
51. Horcas I, et al. WSXM: a software for scanning probe microscopy and a tool for nanotechnology. Rev Sci Instrum. 2007; 78:013705. [PubMed: 17503926]
52. Strohalm M, Kavan D, Novák P, Volný M, Havlíček V. mMass 3: A Cross-Platform Software Environment for Precise Analysis of Mass Spectrometric Data. Anal Chem. 2010; 82:4648–4651. [PubMed: 20465224]
53. Marshall AG, Rodgers RP. Petroleomics: Chemistry of the underworld. Proc Natl Acad Sci. 2008; 105:18090–18095. [PubMed: 18836082]
54. Koch BP, Dittmar T. From mass to structure: An aromaticity index for high-resolution mass data of natural organic matter. Rapid Commun Mass Spectrom. 2006; 20:926–932.

Europe PMC Funders Author Manuscripts

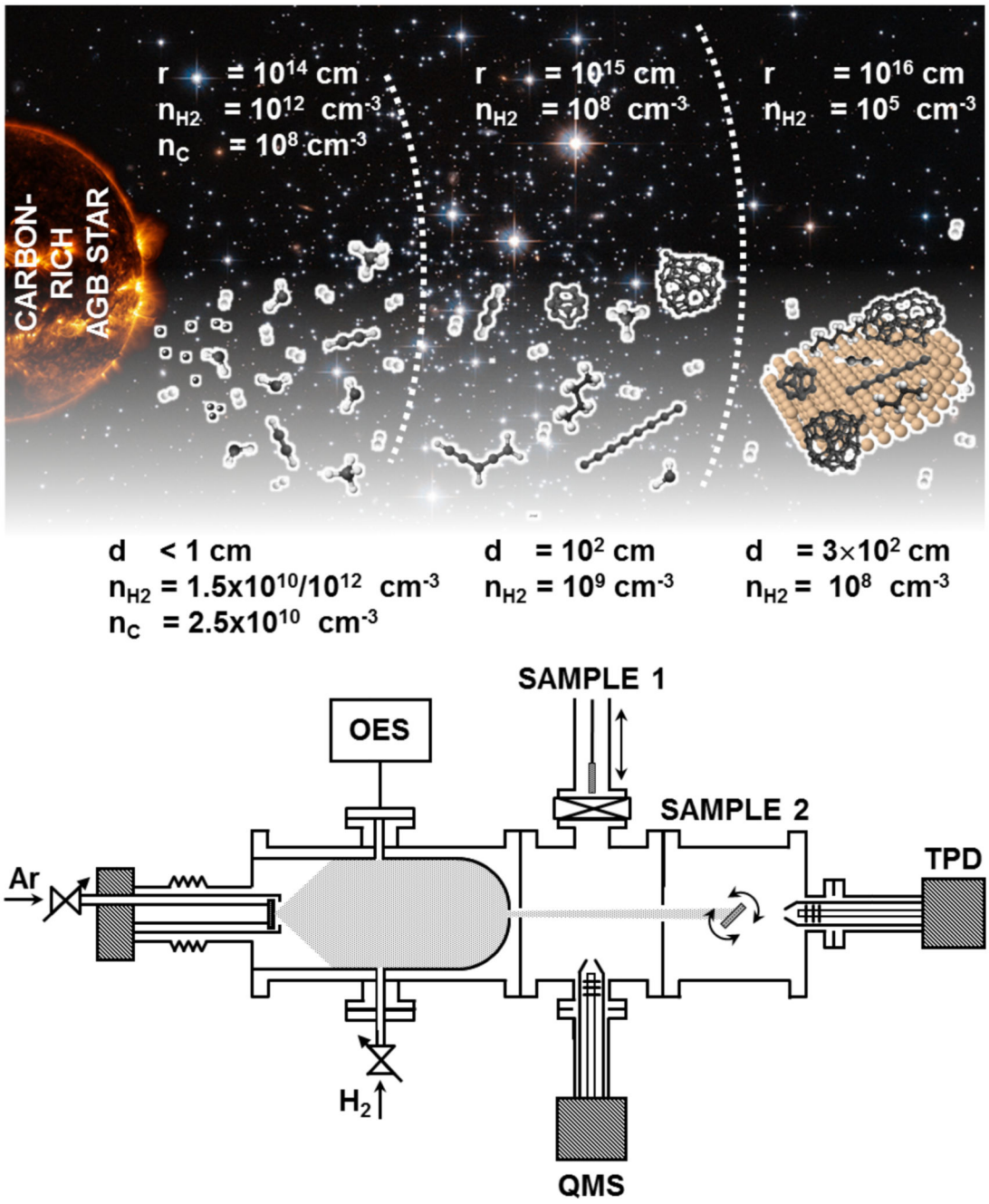

Fig. 1. Production of stardust analogues.

Upper part: pictorial representation of the CSE of a C rich AGB star, with typical carbon and hydrogen densities at given distances provided according to reference[28]. **Lower part:** Schematic of the Stardust machine configuration used in these experiments, considering typical C and H_2 densities. From left to right: there are three different vacuum environments: aggregation zone, where OES measurements are performed and H_2 introduced; expansion area, where the quadrupole mass spectrometer (QMS) is placed and we collect samples for

ex situ studies (sample 1 position), and analysis area (sample 2), where thermal programmed desorption (TPD) is performed.

Europe PMC Funders Author Manuscripts

Europe PMC Funders Author Manuscripts

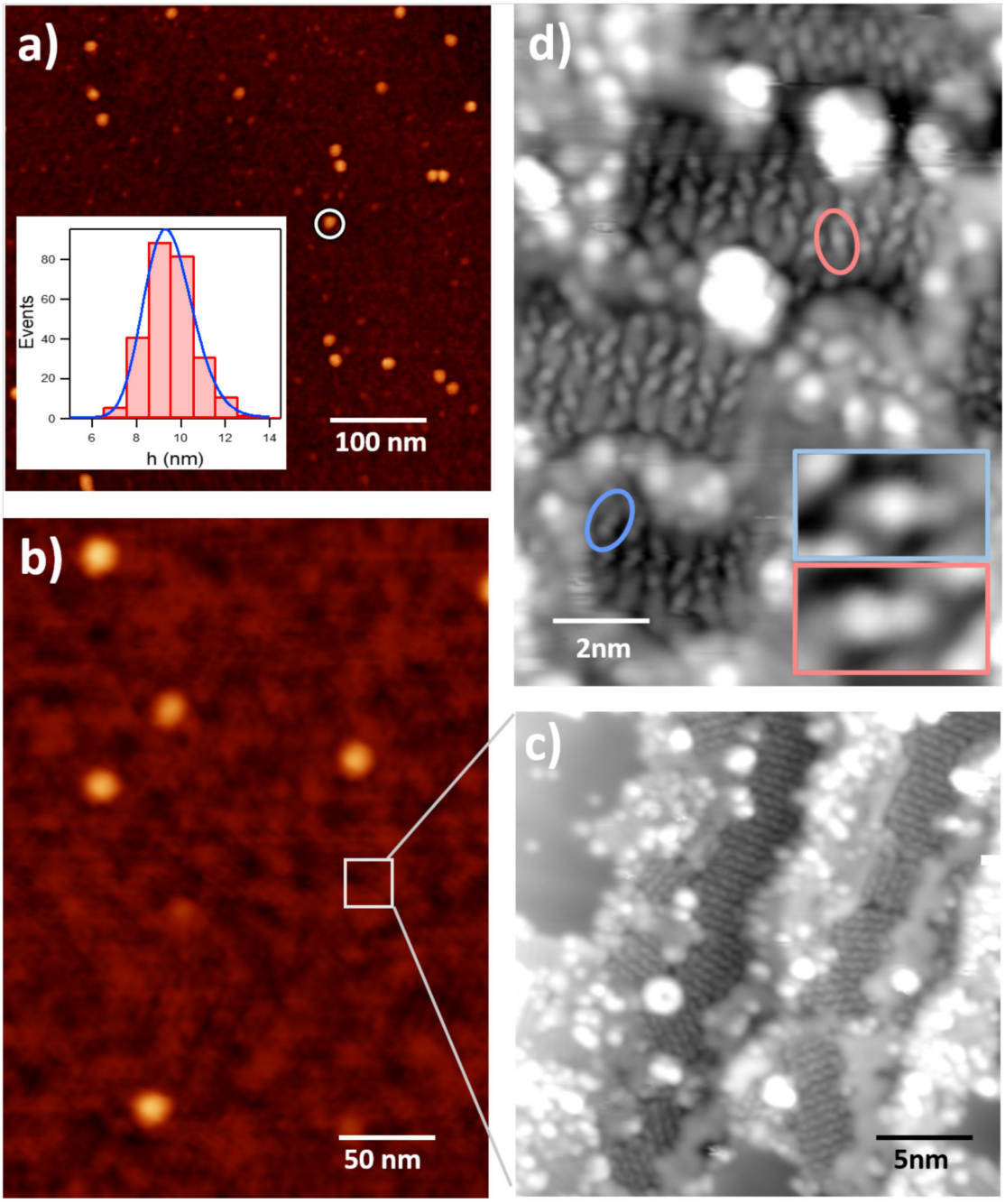

Fig. 2. Production and structure of the stardust analogues.

a-b, AFM images recorded ex situ on a SiO_x surface at the position labelled “sample 1” in Fig. 1, showing the presence of C-nanoparticles and small clusters forming an almost continuous layer. A single nanoparticle is encircled in fig. 2a. Inset of fig. 2a shows the size distribution in a bar-histogram performed over several images. The blue line represents the log-normal fitting of the size distribution **c-d**, in situ recorded STM images of a C-cluster film deposited on a Au surface at “sample 2” position in Fig. 1. Scanned area: 25x25 nm^2, recorded at 50 pA, 1400 mV. Inset: Zoom of the rectangular area 5x3 nm^2, I= 10 pA,

V=1400 mV. Two small molecules are encircled and zoomed in the inset of fig. 2d. The white lines showing the enlarged area in fig. 2b are for clarity and do not correspond to the exact area where measurements were taken. All images were recorded for the case of low-H_2 concentration.

Europe PMC Funders Author Manuscripts

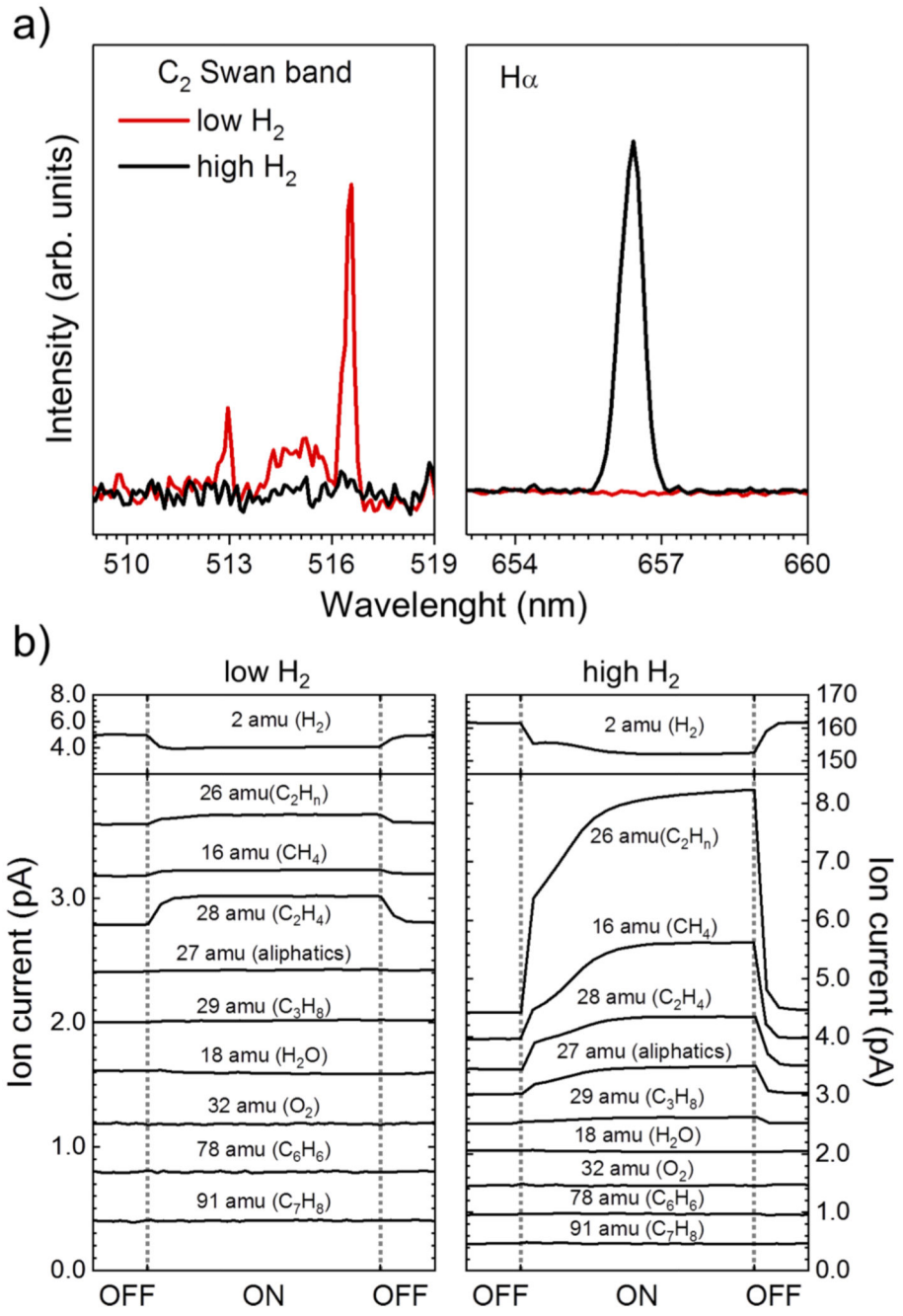

Fig. 3. Spectroscopic characterization of the molecular species.

a, Optical emission spectra recorded at position OES in Fig. 1b for low and high H_2 densities. **b,** In situ gas-phase mass spectroscopy detection at position QMS of most important masses for low and high H_2 densities. Vertical dashed lines indicate the time period where the magnetron was switched on and off. All masses have been offset for clarity.

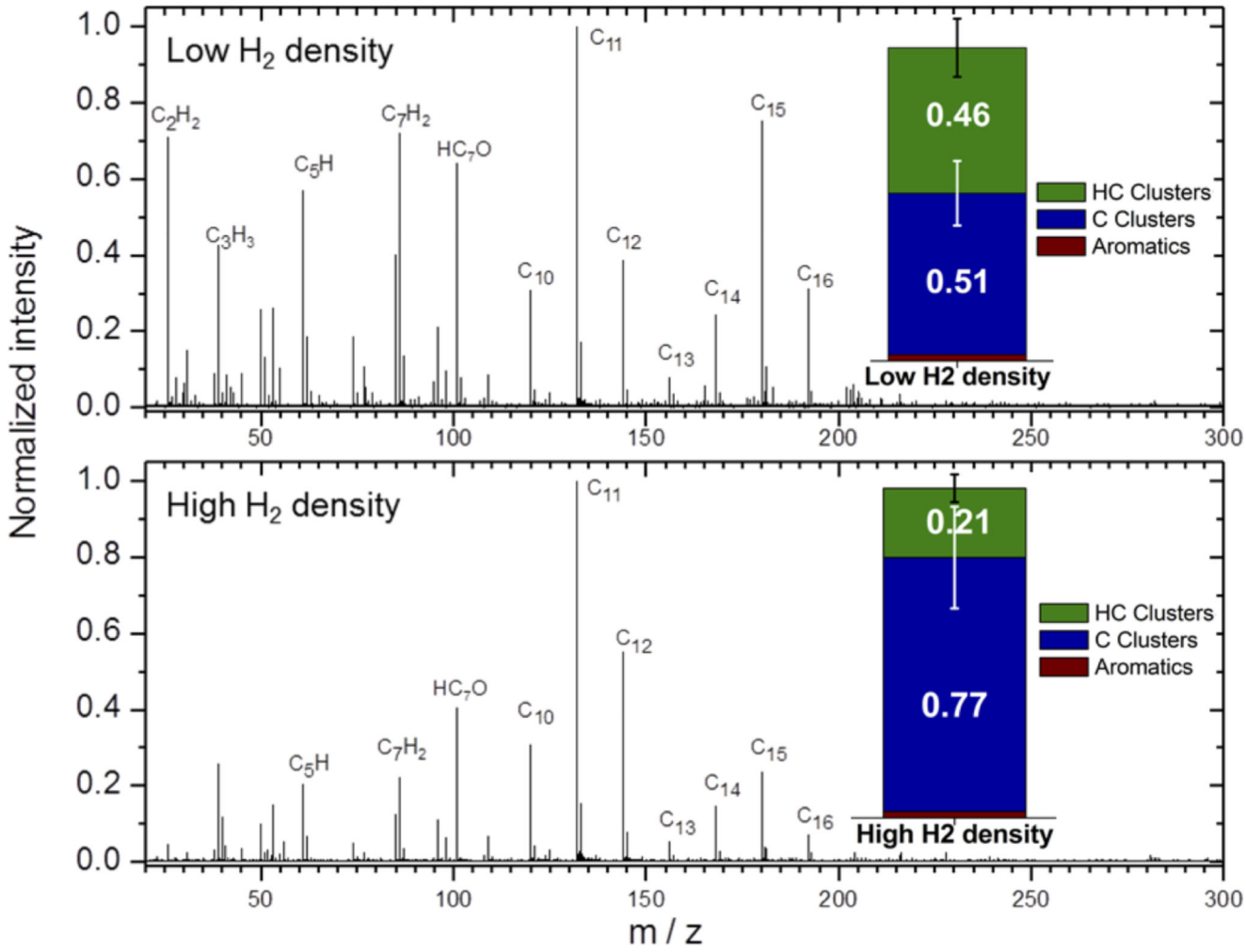

Fig. 4. Ex situ laser desorption/ionization mass-spectrometry (LDI-MS)
from samples grown with a low (upper panel) and high (lower panel) H_2 densities. Data are normalized to the highest peak. Insets: Stacked bar graphs summarizing the family compositions by double bond equivalent (DBE) analysis on the full spectra (see Methods). The error bars correspond to the relative standard deviation obtained for the total ion signal over a mass range for each family of compounds.

Europe PMC Funders Author Manuscripts

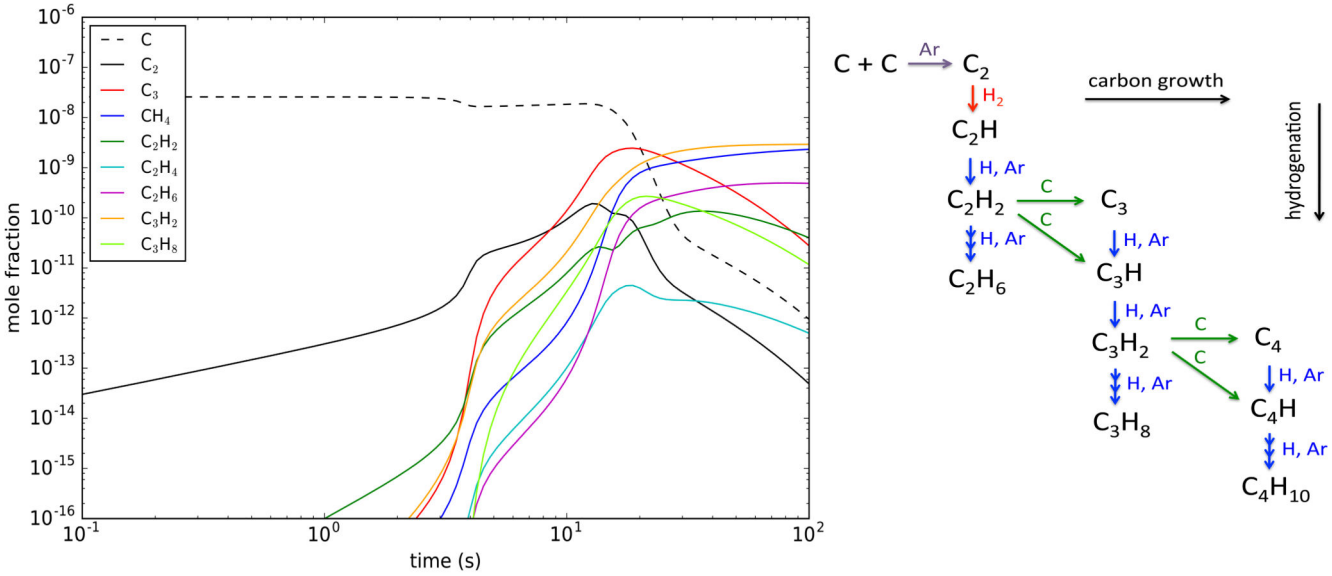

Fig. 5. Computed evolution of the molecular species formed

Left: Evolution of the chemical composition computed with the chemical kinetics model as the gas flows in the aggregation zone, calculated using the values for high hydrogen densities (see text) and at T=500K. Right: Chemical scheme of synthesis of hydrocarbons from atomic carbon given by the chemical kinetics model. Calculations performed for the case of high hydrogen density.

Europe PMC Funders Author Manuscripts

Europe PMC Funders Author Manuscripts

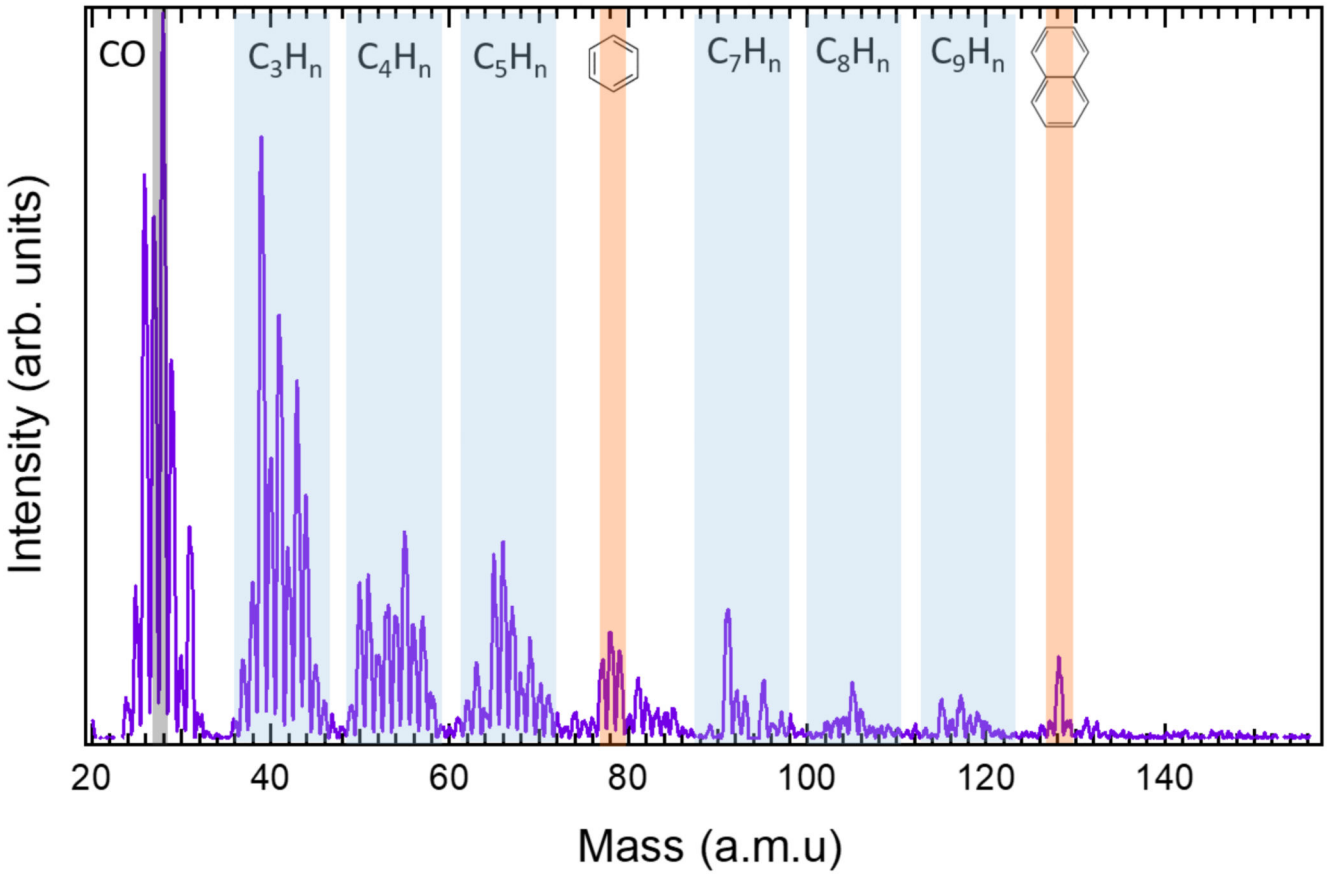

Fig. 6. Representative mass spectrum from a thermal desorption experiment
on C-analogues formed using high H_2 density on a Au surface. Temperature of 430 K. (see full TPD spectra in Supplementary Figure 6).